Applied Catalysis B: Environmental 300 (2022) 120716

Contents lists available at ScienceDirect

Applied Catalysis B: Environmental

journal homepage: www.elsevier.com/locate/apcatb

Promotional effects of sodium and sulfur on light olefins synthesis from syngas over iron-manganese catalyst

Xiaoli Yang [a], Jia Yang [b,*], Yalan Wang [b], Tao Zhao [a], Haoxi Ben [a], Xuning Li [c], Anders Holmen [b], Yanqiang Huang [c], De Chen [b,*]

[a] State Key Laboratory of BioFibers and Eco-textiles , Qingdao University, Qingdao 266071, China
[b] Department of Chemical Engineering, Norwegian University of Science and Technology, Trondheim 7491, Norway
[c] State Key Laboratory of Catalysis, Dalian Institute of Chemical Physics, Chinese Academy of Sciences, Dalian 116023, China

ARTICLE INFO

Keywords:
FTO
$FeMnO_x$ catalyst
Promoters
SSITKA
Kinetic analysis

ABSTRACT

Fischer–Tropsch synthesis of light olefins plays a vital role in the production of major chemical building blocks from non-petroleum resources, having great academic and commercial importance. Herein, Na and S modulated $FeMnO_x$ catalysts were employed to systematically investigate the influence of additives, which not only enhanced the CO conversion but also facilitated the olefin formation and suppressed the undesired methane formation. Multiple characterizations confirmed that the existence of promoters would enhance the formation of active species of Fe_5C_2 at FTO conditions because of the promoted carbon insertion into the iron species from the intermediates dissociation. Combined the steady-state isotopic transient kinetic analysis with dynamic calculation, it confirmed that the promoters indeed had the ability to lower CO activation energy, as well as increase the carbon chain growth activity and the energy barrier to hydrogenation. This study provides a practical strategy for exploring the highly active and stable FTO catalysts.

1. Introduction

Light olefins ($C_{2-4}^{=}$), the key platform molecular in the current chemical industry, are traditionally produced from petroleum refinery processes such as the cracking of hydrocarbons [1,2]. In order to alleviate the dependence on fossil resources, Fisher-Tropsh (FT) synthesis that converts coal/natural gas/ biomass-derived syngas (CO and H_2) into multi-carbon hydrocarbons has been proposed and practiced [3–6]. However, the products are complex since they follow the Anderson-Schulz-Flory distribution governed by a fixed chain growth probability [7–9]. Consequently, the exploration of catalysts with high $C_{2-4}^{=}$ selectivity becomes the top priority.

Among the reported catalysts, Fe-based catalysts not only are promising in the highly selective production of light olefins, but also have broad operation conditions and high tolerance to contaminants, thus gaining great interest [10]. On the other hand, manganese has been widely described as an effective promoter of iron catalysts to enhance olefin selectivity and suppress undesired methane formation [11]. With these regards, FeMn-based catalysts are considered as a potential candidate for catalytic conversion of syngas to olefins, receiving extensive investigations in recent years [12,13]. For example, Al-Sayari et al.[14] explored a series of MnO_2–Fe_2O_3 catalysts, obtaining a CO conversion rate of 15% and an olefins yield of about 23.77%. With the in-situ characterizations, Liu et al.[15] reported that the Mn located on surface of γ-Fe_2O_3 nanorods exhibited low oxidation state due to the strong Fe-Mn interaction, which was beneficial to the formation of C-poor iron carbide species during carburization. This led to an outstanding selectivity of light olefins (61.2%) at CO conversion of 55.1%.

Significantly, other promoters like alkali metals are quite commonly explored as additives in the catalyst design as they could improve the catalytic performance [16,17]. By adding potassium, Graf et al.[18] found that the fast formation channel of CH_4 was blocked and established a slower reaction pathway in the syngas conversion process, resulting in a low CH_4 selectivity. Similarly, Zhai et al.[19] studied that the existence of Na on the iron-based catalyst altered the electronic structure of active sites, suppressing the hydrogenation of double bonds. Notably, de Jong et al.[20] reported the low concentrations of sulfur plus sodium were excellent promoters for Fe/α-Al_2O_3, which obtained a high C_{2-4} olefins selectivity of 50%C and decreased methane production

* Corresponding authors.
E-mail addresses: jia.yang@ntnu.no (J. Yang), de.chen@ntnu.no (D. Chen).

https://doi.org/10.1016/j.apcatb.2021.120716
Received 24 June 2021; Received in revised form 25 August 2021; Accepted 10 September 2021
Available online 14 September 2021

to lower than 20%C under the reaction conditions of 340 °C, 20 bar and $H_2/CO = 1$. Xie et al. [21] further studied the effect of Na and S promoters on the Fe/CNF, finding the CO conversion decreased but the olefin selectivity increased quite a lot. However, their influence and specific roles over $FeMnO_x$ remain unclear.

Here, we prepared the $FeMnO_x$ as catalyst for the conversion of syngas to light olefins. By adding Na and S additives, the catalytic performance was studied to make a comparison. The structural and the dynamically chemical states of two catalysts were examined with multi-techniques. Meanwhile, SSITKA study was conducted to explore the essential nature of changes in performance in terms of the active site and intrinsic activity. By means of kinetic calculation and the analysis of charge change of iron species, a better understanding of the effect of Na and S additives on $FeMnO_x$ catalyst for the light olefin formation was achieved.

2. Experimental methods

2.1. Materials and catalysts synthesis

Iron(III) nitrate nonahydrate, manganese(II) nitrate tetrahydrate, ammonium hydroxide, sodium citrate dehydrate and ferrous sulfate heptahydrate were purchased from Sigma-Aldrich Company Ltd. All chemicals were used as received without further purification.

Fe-Mn oxide was prepared by the co-precipitation method. Briefly, 5.66 g $Fe(NO_3)_3{\cdot}9H_2O$ and 1.51 g $Mn(NO_3)_2{\cdot}4\ H_2O$ were premixed and dissolved into 100 mL H_2O with stirring at 80 °C. Ammonium hydroxide solution (0.25 moL L^{-1}) was then added dropwise to the mixed nitrate solution with continuously vigorous stirring at 80 °C until the pH becoming 9. After aging for 3 h, the resulting solid was recovered by filtration from the suspension, washed with deionized water and dried at 80 °C overnight. For the promoted catalysts, the sodium and sulfur were incorporated into the above solid by incipient-wetness impregnation method. 0.112 g sodium citrate dehydrate and 0.005 g ferrous sulfate heptahydrate were dissolved into the H_2O, which was added into the 1.0 g solid with stirring evenly. After aging at room temperature for 10 h, the mixture was dried at 80 °C overnight. Subsequently, the parent and promoted catalysts were calcined in air at 500 °C for 5 h, which were denoted as $FeMnO_x$ and NaS-$FeMnO_x$, respectively. Elemental content analysis was acquired from EDS (Table S1).

2.2. Activity measurements

The catalytic testing of syngas conversion was carried out in a continuous flow fixed-bed reactor equipped with a K-type thermocouple locating at the center of the catalyst bed. Prior to the activity tests, 500 mg of catalyst powders were pre-reduced in H_2 (20 mL min^{-1}, STP) at 360 °C for 5 h under atmospheric pressure. The catalytic activity was measured under the feed gas of CO/H_2 (1/2, vol%) with Ar as internal standard in the temperature range of 280–320 °C, GHSV of 1600 mL $g_{cat}^{-1}\ h^{-1}$ and atmospheric pressure. The effluent gases after reactions were selectively allowed to pass through an ice-water bath unit and then analyzed online by an Agilent 7890B gas chromatographs. The selectivity of hydrocarbons was calculated excluding CO_2 as reported previously[22]. As previous study showed [9,21], the catalytic performance was expressed as moles of converted CO or the moles of formed hydrocarbons per mole of surface Fe_5C_2 per second (TOF). They were calculated using the density of Fe_5C_2 ($\rho = 7.57$ g mL^{-1}) and assuming there were 75 Fe atoms/nm^3 and 17.8 Fe atoms/nm^2. Combined with the XRD patterns, EDS and Mossbauer analysis, the particle sizes of Fe_5C_2, the content of iron and iron carbide could be obtained. The carbon balance was over 90% based on the result of detected products.

For SSITKA experiments, 200 mg $FeMnO_x$ or 100 mg NaS-$FeMnO_x$ powders mixed with SiC were weighed as catalysts to control the conversion between 10% and 15%, which were better to calculate the surface residence time (τ_i) and surface concentration (N_i) of intermediates. After in-situ reduction in H_2/Ar flow (20/5 mL min^{-1}) at 360 °C for 5 h and subsequent cooling in Ar (25 mL min^{-1}), the feed of $^{12}CO/H_2/Ar$ (0.75/7.5/16.75 mL min^{-1}, 0.18 MPa) was introduced for CO hydrogenation at 320 °C. The isotopic transients switch from $^{12}CO/H_2/Ar$ to $^{13}CO/H_2/Kr$ was conducted after 10 h on stream during a relatively stable reaction period. A combined GC-MS and a separate mass spectrometer (MS) were used to collect the signals of isotopic transient response and calculate conversion and selectivity [23,24].

2.3. Catalyst characterizations

Powder X-ray diffraction (XRD) patterns were recorded on a Bruker D8 Advance diffractometer equipped with Cu Kα radiation source ($\lambda = 0.15432$ nm, 40 kV, 40 mA). The scanning electron microscopy (SEM) images and elemental mapping of the catalysts were obtained on JSM-6390LV microscope equipped with EDX analyzer. N_2 physisorption was conducted on an ASAP 2460 Quantachrome instrument to obtain the surface area and pore volume of the samples. Before analysis, the samples were degassed in vacuum for 5 h at 200 °C.

Temperature programmed reactions were conducted on a Micromeritics AutoChem II 2920 apparatus. For H_2-TPR measurements, the samples were pretreated under Ar flow at 200 °C for 1 h. After cooling to 50 °C, 10 vol% H_2/Ar was introduced to pass through the sample while being heated to 800 °C with a ramping rate of 10 °C min^{-1}. On the other hand, the CO chemisorption at 50 °C was conducted after the in-situ reduction at 360 °C for 5 h under 10 vol% H_2/Ar flow. Moreover, temperature-programmed desorption of H_2 (H_2-TPD) was performed after the in-situ reduction and subsequent H_2 adsorption saturation, the pre-treated samples were set in He flow (20 mL min^{-1}) and heated from 100 °C to 800 °C at a ramping rate of 10 °C min^{-1}.

X-ray photoelectron spectra (XPS) were acquired on a VG ESCALAB 210 apparatus with Al Kα ($h\upsilon = 1486.6$ eV) as the X-ray source, and the core-level spectra of Fe2p and Mn2p were collected. Spectra were referenced to the valence band of C1s peak at 284.8 eV binding energy (BE). The X-ray absorption spectra(XAS) including X-ray absorption near-edge structure(XANES) and extended X-ray absorption fine structure (EXAFS) of the samples at Fe K-edge (7112 eV were collected at the Singapore Synchrotron Light Source(SSLS) center. The output beam was selected by Si (111) monochromator with a Fe foil employed for energy calibration. Athena software package was employed to process the XANES data. Transmission ^{57}Fe Mössbauer spectra were collected at room temperature on a Topologic 500 A spectrometer, using ^{57}Co(Rh) as a radioactive source that moved in a constant acceleration. The obtained spectra were fitted based on a Lorentzian line shape to determine the parameters including isomer shift (IS) and quadrupole splitting (QS). The IS values and Doppler velocities were calibrated by a standard α-iron foil. Notably, the catalysts were activated through pre-reduced at 360 °C for 5 h prior to the above measurements.

3. Results and discussion

3.1. Catalytic properties for syngas conversion

Fig. 1a displayed the catalytic performance of syngas conversion over $FeMnO_x$ and NaS-$FeMnO_x$ at 280 °C. It was observed that the product distribution showed obvious differences. With regard to $FeMnO_x$ catalyst, the CH_4 and C_{2-4} alkanes occupied a large part of the products (20% and 21%), while they respectively decreased to 5% and 4% over NaS-$FeMnO_x$ catalyst. In contrast, the selectivity of C_{2-4} alkenes grew from 5% to 18%, and the olefin to paraffin (o/p) ratio for C_{2-4} significantly increased from 0.24 to 4.5 over the promoted catalyst. The hydrocarbons with long carbon chain (C_5^+) also revealed an increase trend, the estimated carbon chain growth probability increased from 0.25 on $FeMnO_x$ to 0.34 on NaS-$FeMnO_x$. Besides, the stable CO conversion increased from 10% over the un-promoted catalyst to 19% over the promoted catalyst, unambiguously illustrating that the presence of

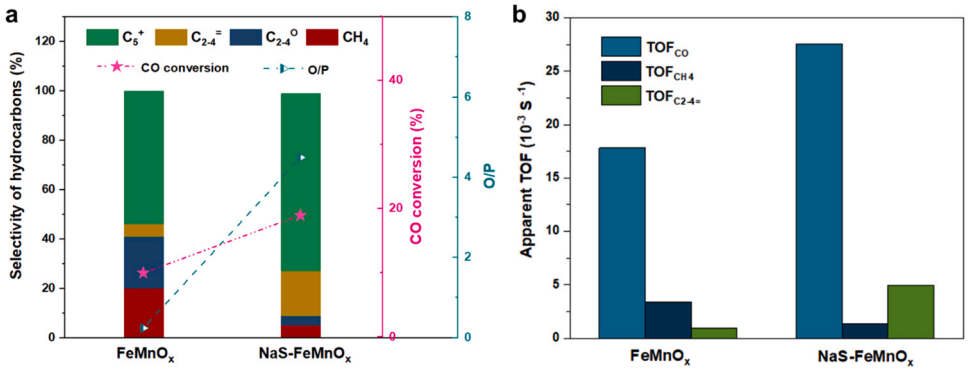

Fig. 1. (a) Catalytic performance and (b) apparent TOF over two catalysts at 280 °C, 1600 mL g_{cat}^{-1} h^{-1} and atmospheric pressure (H_2/CO/Ar= 6/3/1).

Na and S facilitated the enhancement of CO conversion. This was different from the situation of Fe/CNF, which the CO conversion decreased after adding the Na and S promoters [21]. Additionally, similar changes in the activity and product selectivity were also observed at 320 °C (Fig. S1 and Table S2). All of these elucidated the positive role of promoters in the improvement of CO conversion and olefin formation, as well as the suppression of undesired products like methane and C_{2-4} alkanes.

Further calculating the apparent TOF to explore the intrinsic effect of promoters, it was found that the TOF of CO was 0.018 s^{-1} for FeMnO$_x$, while that for NaS-FeMnO$_x$ was 0.028 s^{-1}, which was much higher than the parent catalyst (Fig. 1b). Apart from that, the CH_4 formation rate also decreased from 0.0034 to 0.0014 s^{-1}, but the C_{2-4} alkenes drastically climbed from 0.0009 s^{-1} to 0.0050 s^{-1}. The notable difference in the formation rates implied that Na and S promoters would alter the activity of catalytic sites for the selective conversion of syngas into light alkenes over FeMnO$_x$ system.

3.2. Steady state isotopic transient kinetic analysis (SSITKA)

Steady state isotopic transient kinetic analysis (SSITKA) allows to measure kinetic parameters, including the concentration of surface intermediates, surface residence time and intrinsic rate constant. Since the catalytic performance mainly influenced by the intrinsic activity of active sites and the number of adsorption sites, the nature of the enhancement of catalytic performance by the promoters can be analyzed by means of SSITKA [25–27]. CO hydrogenation was studied at a methanation condition with a high H_2/CO ratio of 10. As shown in the Table 1, the CO conversion rate of NaS-FeMnO$_x$ was 0.69 μmol g_{cat}^{-1} s^{-1}, which was more than twice that of FeMnO$_x$ (0.33 μmol g_{cat}^{-1} s^{-1}). Besides, Fig. 2c showed the products were mostly terminated as methane on FeMnO$_x$, while they moved to longer chain hydrocarbons on NaS-FeMnO$_x$, indicating the chain growth probability was significantly enhanced by the promoters.

Based on further quantitative calculation of the normalized transient response of Ar, CO and CH_4 over two catalysts in Fig. 2a–b, it was found that the surface CO concentration (N_{CO}) of NaS-FeMnO$_x$ was higher than that of FeMnO$_x$ under reaction conditions. Notably, the residence time of CO on FeMnOx was about 22 s while the one on Fe/CNT was close to zero where the CO and Ar transient curves overlap [21]. It suggested CO dissociation rate were lower over the FeMnO$_x$ system. This might be the reason that the trend of CO conversion in FeMn and Fe catalysts was different after adding Na and S additives. Whereas, the surface concentration of CH_x intermediates that led to CH_4 (N_{CHx}) decreased by almost five times over NaS-FeMnO$_x$ (1.8 μmol g_{cat}^{-1}, vs 8.8 μmol g_{cat}^{-1} over FeMnO$_x$), indicating lower surface coverage of H atoms in the presence of promoters. In addition, the mean resident time of CO was significantly lower over the NaS-FeMnO$_x$ than that on the FeMnO$_x$, so as with the mean resident time of intermediates. Assuming this process as first-order reaction, the intrinsic rate constant of CO hydrogenation to methane can be calculated by using the reciprocal of the average surface residence time for the active surface ($k = \tau^{-1}$) [28,29]. Thus, the CO conversion rate constant of NaS-FeMnO$_x$ was 0.083 s^{-1}, while that of the FeMnO$_x$ was only 0.045 s^{-1}. Similarly, the intrinsic rate constant of forming intermediates was 0.077 s^{-1} on NaS-FeMnO$_x$, much greater than that over FeMnO$_x$ (0.019 s^{-1}). The rate constant on NaS-FeMnO$_x$ was about a few times of that on FeMnO$_x$.

These results revealed that the Na and S promoters had the following functions: 1) enhanced CO adsorption; 2) lowered the amount of intermediate leading to methane; 3) significantly enhanced the intrinsic CO hydrogenation rate and 4) enhanced the chain growth rate. To make the promotional role clearer, the discussion based on the above characterizations were thoroughly revealed as follows.

3.3. Catalyst characterizations

3.3.1. The catalyst structure

The structural changes were analyzed by SEM, N_2 physical sorption and XRD to assess the impact of additive Na and S promoters upon FeMnO$_x$ catalysts. According to the morphologies and EDS mappings (Figs. S2–3 and Table S2), the particle size of NaS-FeMnO$_x$ was a little smaller. In addition, Fe and Mn species were evenly distributed in both fresh catalysts, and the promoters were also homogeneously dispersed on the promoted catalyst. As for the surface area and pore volume, NaS-FeMnO$_x$ showed a decreased trend than the parent FeMnO$_x$ as a result of the additional elements (Table S3 and Fig. S4). From the Fig. S5, unpromoted and promoted catalysts exhibited the same XRD pattern, both of which existed in the form of Fe_2O_3 and $FeMnO_3$ [30,31]. However, for the catalysts after reduction, there appeared peaks with completely different positions and intensities (Fig. S6). After analyzing the spectrum, it was found that the peaks of two catalysts were attributed to iron oxide, but the valence state of iron on the NaS-FeMnO$_x$ catalyst was lower. These all implied there might be more catalytic sites over the promoted catalyst since iron species was acting as the active

Table 1
The SSITKA parameters over FeMnO$_x$ and NaS-FeMnO$_x$ catalysts.

Samples	R_{CO} [μmol g_{cat}^{-1} s^{-1}]	R_{CH4} [μmol g_{cat}^{-1} s^{-1}]	N_{CO}[μmol g_{cat}^{-1}]	N_{CHx} [μmol g_{cat}^{-1}]	τ_{CO} [s]	k_{CO} [s^{-1}]	τ_{CHx} [s]	k_{CHx} [s^{-1}]
FeMnOx	0.33	0.16	52.8	8.8	22	0.045	53	0.019
NaS-FeMnOx	0.69	0.11	54.2	1.8	12	0.083	13	0.077

Reaction conditions: $^{12}CO/H_2/Ar$ (0.75/7.5/16.75 mL min^{-1}), 0.18 MPa, 320 °C.

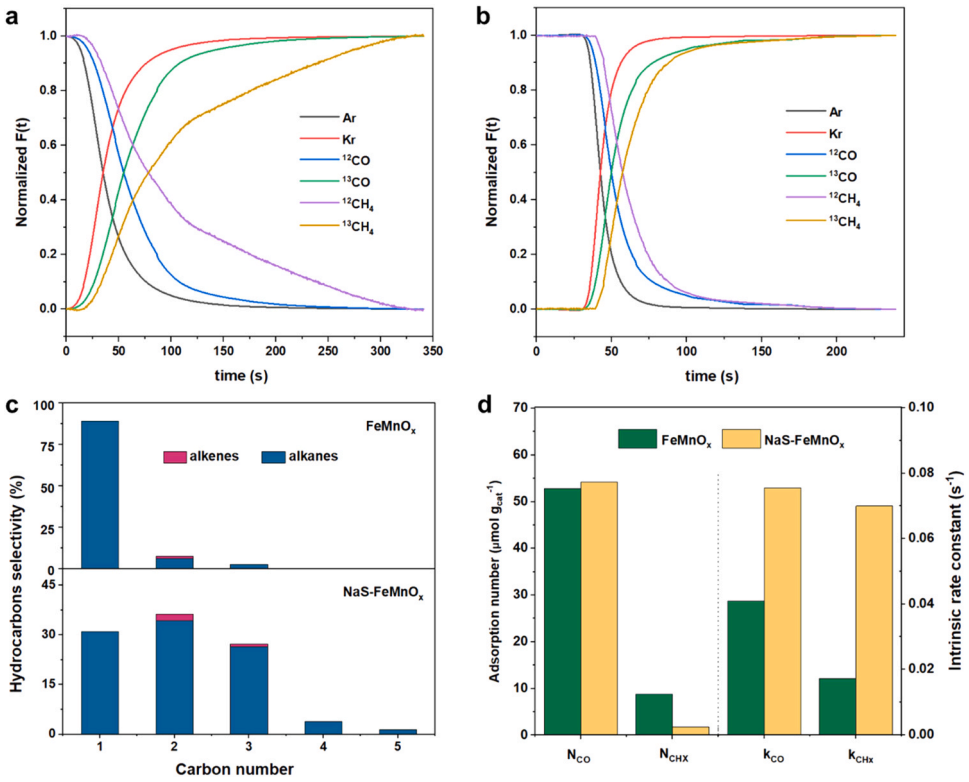

Fig. 2. Normalized transient curve of SSITKA experiments over (a) $FeMnO_x$ and NaS-$FeMnO_x$ catalysts. (c) Alkanes and alkenes distribution with different carbon number on two catalysts. (d) Adsorption amount of CO and intermediates over two catalysts.

parts [14].

3.3.2. *The chemical state of iron species*

Considering the intrinsic activity were affected by the electronic properties of active species, the electronic state of two catalysts were tested here to explore the changes in catalytic sites. As shown in Fig. 3a, H_2-TPR curves of both two catalysts displayed four peaks, which could be attributed to the reduction of $FeMnO_x$ to Fe_3O_4 and MnO, then reduction to FeO and further to metallic Fe, respectively [32]. However, it was noted that all the peaks shifted to a higher temperature over NaS-$FeMnO_x$, suggesting that the presence of promoters would enhance the FeMn interaction and then suppress the reduction of iron oxides [33]. The alteration in the chemical states of surface iron and manganese species due to the promoters was investigated by XPS analysis, as displayed in Fig. 3b–c. Observing the spectra of Fe_{2p}, the peak attributed to metallic iron in the $FeMnO_x$ catalyst surprisingly disappeared after adding promoters. In addition, the area of iron signal at about 710.2 eV which attributed to iron oxide clearly increased but that of manganese signal decreased after the addition of promoters. It meant more catalytic sites exposed on the surface in the reduced NaS-$FeMnO_x$ catalyst [34], and there existed electron transfer between the promoters and iron species to modulate their electronic states [35,36].

To accurately acquire the status of iron species in the reduced catalysts, Mössbauer spectroscopy that has a better sensitive and quantitative analysis for Fe species was employed here [37,38]. In Fig. 3d–f and Table S4, Fe_3O_4, FeO and Fe species were found over both catalysts. Whereas, the metallic Fe occupied the major part over $FeMnO_x$, about 66.32%, but FeO accounted for 62.1% over NaS-$FeMnO_x$. These phenomena were a manifestation of the electronic effect of the Na and S additives, which suppressed the reduction of FeO to Fe. In view of the study of Weckhuysen et al. [39] that the slight changes in local oxidation state of cobalt would affect the heterogeneities of catalysts and the further hydrocarbon build-up, the change of iron species here should also be related to the chemical state and therewith affect the reaction process.

The chemical states of iron species over two catalysts after 10 h reaction was thus studied. The surface species was under a stable state and the catalyst chemical state was believed to be rather close to the working surface. The element contents were firstly analyzed to show that there contained carbon over both catalysts, implying the possible formation of carbonized species. While, the carbon content was much higher on the NaS-$FeMnO_x$ (Table S5). From the XRD patterns (Fig. S7), it showed the peaks of iron oxide and iron carbide over both catalysts. Notably, the peaks of iron carbide were much obvious over NaS-$FeMnO_x$. After analysis, it revealed that the particle size of Fe_5C_2 was about 29.5 nm for $FeMnO_x$ and 32.6 nm for NaS-$FeMnO_x$. Fe k-edge X-ray absorption near edge structure (XANES) spectra of the two catalysts in Fig. 4a showed that the oxidation state of Fe in NaS-$FeMnO_x$ treated at the CO hydrogenation reaction condition was lower than that in $FeMnO_x$. The extended X-ray absorption fine structure (EXAFS) spectra of two samples (Fig. S8) both exhibited Fe-C (~2.0 Å) and Fe-Fe (~2.5 Å) scattering signals from the FeC_x phase [40,41], but at different specific positions, which might be caused by the in-situ formation of different types of iron-carbon bonds during reactions (Table S6). Further observing from the Mössbauer spectroscopy, the content of different types of iron species were estimated in Fig. 4b-d and Table S7. Both samples contained Fe_3O_4, FeO and three types of Fe_5C_2, illustrating the co-exist of iron oxides and iron carbide on the catalyst surface. While, the total iron carbides content in the NaS-$FeMnO_x$ was 71%, much higher than that in the $FeMnO_x$, about 44%, which suggested that the carburization of the catalysts was enhanced over NaS-$FeMnO_x$.

3.4. *The promotional roles*

3.4.1. *The influence of promoters on the Fe_5C_2 species*

The characterizations displayed intuitively that the Na and S promoters have changed the catalyst composition, structure and electronic properties at the working conditions. Significantly, Mössbauer

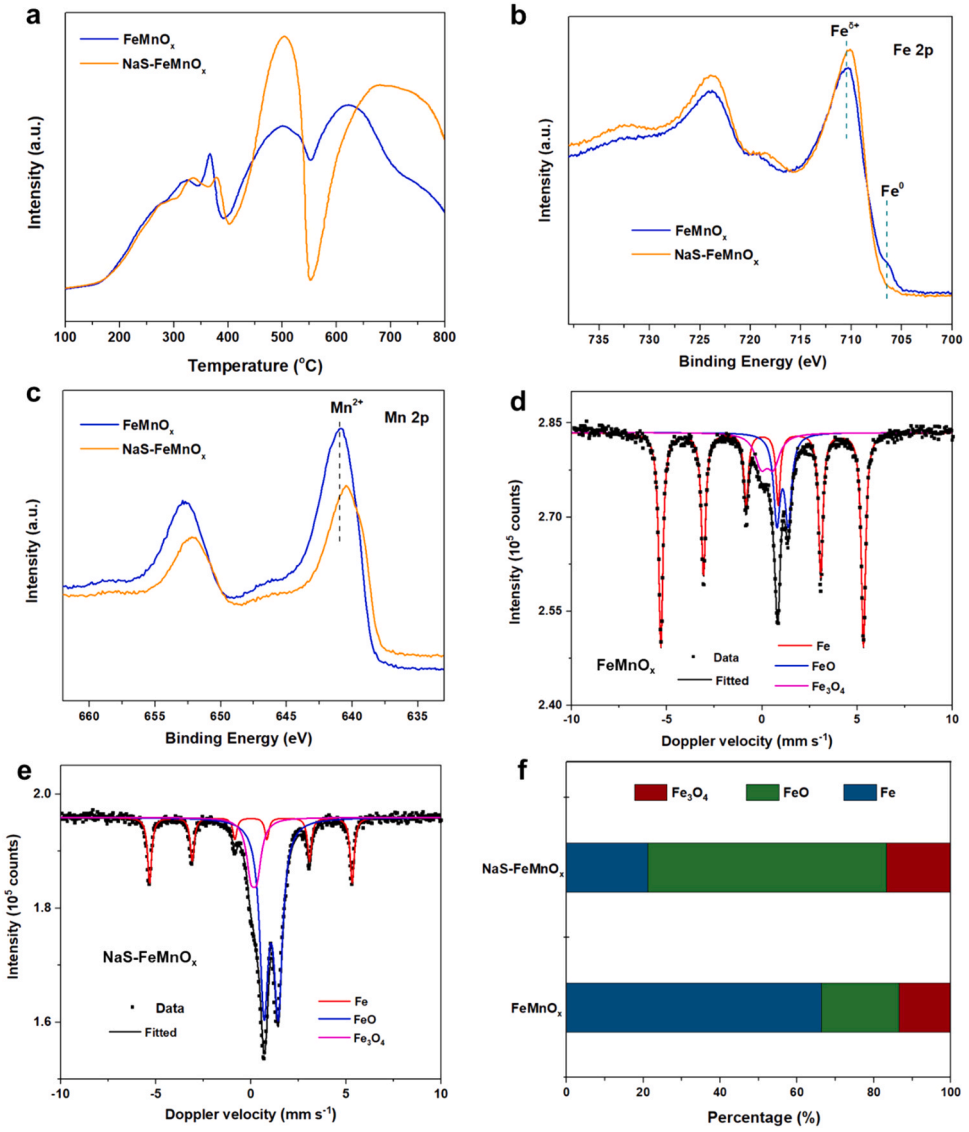

Fig. 3. (a) H_2-TPR curves over two catalysts under 10 vol%H_2/Ar with 20 mL min^{-1}, heating rate: 5 °C min^{-1}. (b) Fe_{2p} and (c) Mn_{2p} X-ray photoelectron spectra of two catalysts after reduction. Mössbauer spectroscopy of (d) $FeMnO_x$ and (e) NaS-$FeMnO_x$ after reduction. (f) The composition of iron species over two catalysts from Mössbauer.

spectroscopic results indicated that Fe_5C_2 occupied the dominating type of carbides on both catalysts, which was the key active phase for CO hydrogenation [42–45]. However, the promoted catalyst kept a much higher concentration of Fe_5C_2 at the steady-state conditions. Since the active sites were highly dynamic during the pretreatment and reaction processes, the higher fraction of Fe_5C_2 cannot be simply explained by the ability of carburization of Fe. It should be firstly noted that the reduction at 360 °C for 5 h under 10 vol% H_2/Ar flow was not able to sufficiently reduce Fe oxides, so the CO/H_2 mixture would further reduce the Fe oxides and carbonize Fe species at the same time. Besides, it was believed that the reaction followed Mars van Krevelen mechanism where the lattice C participated in the reaction [46,47]. That meant there were several reaction steps involved the redox cycle associated with Fe site, including surface carbon formation, carburization of Fe, insertion of surface carbon into the hydrocarbon chain, adsorption and oxidize Fe, and CO oxidation by lattice O or hydrogenation of Fe oxide to form water. The content of FeO_x would depend on the relative hydrogenation and oxidation rates of iron species by surface oxygen, while the FeC_x amount would depend on the relative insertion and removal rates of lattice carbon. Thus, the larger fraction of FeC_x on NaS-$FeMnO_x$ catalyst at FTO reaction conditions compared to un-promoted catalyst suggested that the promoters suppressed the relative oxidation cycle and/or promoted the insertion of carbon that formed by the intermediate's dissociation, which was also in accordance with the fact that the reduction of iron oxide was suppressed over the reduced NaS-$FeMnO_x$.

On the other hand, the normalized site time yield of CO conversion based on the measured surface Fe_5C_2 concentration of 0.028 s^{-1} on NaS-$FeMnO_x$ was higher than $FeMnO_x$ (0.018 s^{-1}). It implied that the promoters did not only increase the active site number but also the site activity, which could be a result of altered surface structure and electronic properties. The XANES analysis pointed a lower white line and a lower oxidation state of Fe on the promoted catalyst after reaction (Fig. 4a). Typical atomic charges at the surface were approximately + 0.15 for Fe and − 0.15 for C, but the charge on nearest Fe neighbors of Na would be lowered by 0.05–0.1e by the local donation of Na [21]. Moreover, the electronic properties also depended on the Fe-C bond length. Based on the Table S6, the Fe-C bond was about 2.00 Å on NaS-$FeMnO_x$, while it was about 2.09 Å on $FeMnO_x$. The compact Fe-C bond over promoted catalyst resulted in a more significant electron

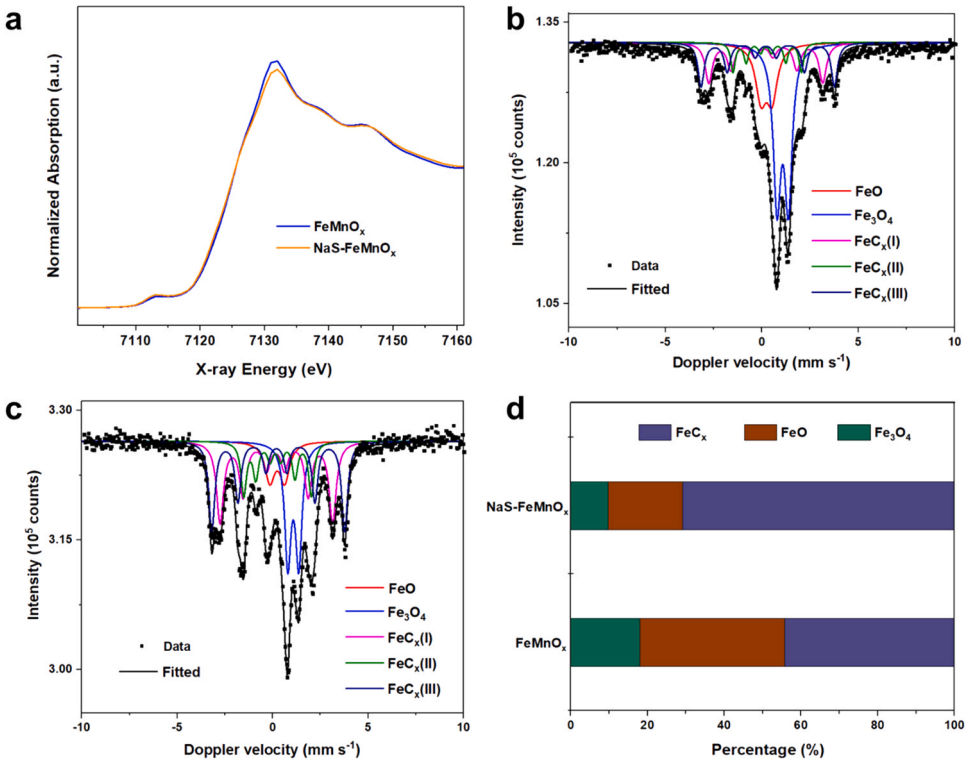

Fig. 4. (a) Normalized XANES spectra at Fe K-edge of two catalysts after reactions. Mössbauer spectroscopy of (b) $FeMnO_x$ and (c) $NaS\text{-}FeMnO_x$ after reaction. (d) The composition of iron species over two catalysts after reaction.

transfer between Fe and C, thus caused a d-bond shift of Fe. DFT study revealed that the most stable Fe-C bond for CO adsorption significantly depended on the facets exposed, such as 1.86 Å on (110), 2.07 Å on (510), 2.10 Å on (311) and 2.14 Å on (001) [42]. A scaling relationship was found between the CO dissociation energy and the Mulliken charge of Fe on Fe_5C_2 with different terminations, vacancies and promoters, and a lower charge was corresponding to a low CO activation energy. It cannot be excluded that the promoters could cause the expose of Fe_5C_2 with different facets compared to the un-promoted catalyst. Anyhow, the increased Fe_5C_2 content, compact Fe-C bond and lower Fe charge rationalized the higher CO conversion activity of $NaS\text{-}FeMnO_x$ under various conditions (Table S8).

3.4.2. Kinetic calculation

The SSITKA study further unraveled the promoters affected on CO hydrogenation to olefins. The surface concentration of adsorbed CO was only slightly higher on $NaS\text{-}FeMnO_x$ under reaction conditions. However, the rate contact k_{CO} was much higher on $NaS\text{-}FeMnO_x$ than on $FeMnO_x$, which was consistent with the results at high pressures. The higher activity was obviously a result of the increased active phase concentration and the electronic promotion of the active sites as discussed above. The most significant effect of the promoters was on the selectivity of methane, C_1-C_4 paraffins and olefins. According to the previous study, the chain initiation, growth and termination in FTO followed a mechanism as shown in Scheme 1, where C_n * was the surface intermediates with carbon number of n [29].

The formation rate of methane ($r_{p,1}$) and the chain growth rate from C1 ($r_{g,1}$) are described by Eqs. (1) and (2), respectively:

$$r_{p,1} = k_{p,1} N_{CHx} N_H^n$$

$$r_{g,1} = k_{g,1} N_{CHx} N_{C*}$$

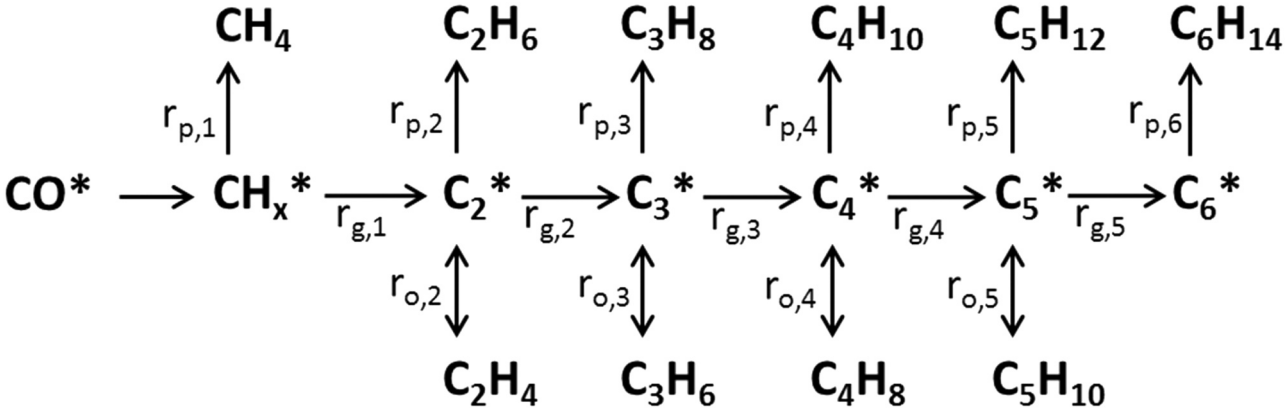

Scheme 1. Reaction network of CO hydrogenation, where the rates for chain growth and termination to paraffin and olefin are marked for each intermediate. (ref. [29]).

where $k_{p,1}$ and $k_{g,1}$ are rate constants, N_H is the surface concentration of adsorbed H, n is the reaction order of H for methane formation, N_{CHx} is the surface concentration of intermediates leading to methane formation, and N_{C*} is the concentration of chain growth intermediates. The chain growth rate of C1 ($r_{g,1}$) can be estimated by $r_{CO} - r_{p,1}$. The chain growth ratio of C1 can be described in Eq. (3):

$$\frac{r_{g,1}}{r_{p,1}} = \frac{k_{g,1}N_{C*}}{k_{p,1}N_H^n} = \frac{k_{g,1}N_{C*}}{k_1} = \frac{k_{g,1*}}{k_1}$$

The chain growth ratio of C1 was estimated to 5.27 on NaS-$FeMnO_x$ based on rates obtained by SSITKA (Table 1), which was remarkably higher than 1.06 on $FeMnO_x$. k_1 was the rate constant measured by SSITKA. $k_{g,1*}$ was the apparent rate constant of chain growth, which was estimated to be 0.406 s^{-1} on NaS-$FeMnO_x$ and 0.02 s^{-1} on $FeMnO_x$. That meant the promoters significantly enhanced the chain growth activity, possibly through enhancing the formation of chain growth intermediate (N_{C*}).

Besides, the olefin to paraffin ratio can be described by the ratio of the formation rate of olefin and paraffin with carbon number of n in Eq. (4):

$$\frac{r_{n,o}}{r_{n,p}} = \frac{k_{n,o}}{k_{n,p}N_H^n}$$

where $k_{n,o}$ and $k_{n,p}$ are the rate constant of olefins and paraffin formation with a carbon number of n. The olefin to paraffin ratio, for example, the ethylene/ethane ratio, was much higher on the NaS-$FeMnO_x$ (2.72) than $FeMnO_x$ (0.01). According to the H_2-TPD curves (Fig. S9), the integral area of $FeMnO_x$ was bigger than that of NaS-$FeMnO_x$, suggesting the H_2 adsorption amount dropped after adding the promoters. Especially, the H_2 adsorption at the reaction temperature (<320 °C) was obviously weak on NaS-$FeMnO_x$. In addition, the location of H adsorption was shown to correlate with the atomic charge of the accepting Fe or C on the Fe_5C_2. With the negative charge donation from the promoters increasing, H adsorption would become stronger on Fe and weaker on C [21]. Thus the H atoms would bind preferably on C after dissociation on Fe for the un-promoted Fe_5C_2 surfaces, while the difference between adsorption on Fe or C became smaller for the promoted Fe_5C_2 surfaces. Combing the statements, it could be concluded that promoters weakened the hydrogen adsorption and also increased the energy barrier to hydrogenation. All of these resulted in less methane formation and more β-H removal leading to olefin formation.

4. Conclusion

The influence of Na and S additives on the catalytic performance in $FeMnO_x$ catalyst for FTO was studied in detail by multiple characterization and SSITKA techniques. Results indicated both the active sites and intrinsic activity changed after the addition of Na and S. On the one hand, the promotes facilitated the formation of more active species of Fe_5C_2 by suppressing the relative oxidation cycle of iron and enhancing the insertion of carbon that formed from the intermediate's dissociation into iron atoms. On the other hand, the existence of electron transferred from promoters reduced the charge of iron and caused more compact bonds of Fe-C, lowing the CO activation energy. Thus, the CO conversion promoted greatly as a comprehensive consequence. Besides, the kinetic calculation based on the SSITKA results indicated that the chain growth activity increased obviously over the promoted catalyst. Also, the olefin formation rate enhanced due to the negative charge donation from promoters, which decreased the H_2 adsorption amount and weakened the adsorption of H atoms on C of Fe_5C_2 during the reaction process. These led to an obvious decrease in methane formation and an increase in the olefin formation. Consequently, the CO conversion and olefin selectivity increased quite a lot on promoted catalysts under various reaction conditions. This study provides some insights into the role of promotes for the FT synthesis, further helping the rational design of catalysts.

CRediT authorship contribution statement

Xiaoli Yang: Conceptualisation, Data curation, Investigation, Formal analysis, Visualization, Writing – original draft. **Jia Yang:** Methodology, Data curation, Writing – review & editing. Yalan Wang: Data curation. **Tao Zhao:** Formal analysis. **Haoxi Ben:** Methodology, Supervision. **Xuning Li:** Formal analysis. **Anders Holmen:** Methodology, Supervision. **Yanqiang Huang:** Conceptualisation, Methodology, Supervision. **De Chen:** Conceptualisation, Methodology, Supervision, Writing – review & editing.

Declaration of Competing Interest

The authors declare that they have no known competing financial interests or personal relationships that could have appeared to influence the work reported in this paper.

Acknowledgements

The authors gratefully acknowledge the National Natural Science Foundation of China (No. 22002066), State Key Laboratory of Bio-Fibers and Eco-Textiles in Qingdao University (No. G2RC202021) for support.

Appendix A. Supporting information

Supplementary data associated with this article can be found in the online version at doi:10.1016/j.apcatb.2021.120716.

References

[1] Z. Li, L. Zhong, F. Yu, Y. An, Y. Dai, Y. Yang, T. Lin, S. Li, H. Wang, P. Gao, Y. Sun, M. He, Effects of sodium on the catalytic performance of CoMn catalysts for fischer-tropsch to olefin reactions, ACS Catal. 7 (2017) 3622–3631, https://doi.org/10.1021/acscatal.6b03478.

[2] F. Jiao, J. Li, X. Pan, J. Xiao, H. Li, H. Ma, M. Wei, Y. Pan, Z. Zhou, M. Li, Selective conversion of syngas to light olefins, Science 351 (2016) 1065–1068, https://doi.org/10.1126/science.aaf1835.

[3] M.E. Dry, High quality diesel via the Fischer-Tropsch process - a review, J. Chem. Technol. Biotechnol. 77 (2002) 43–50, https://doi.org/10.1002/jctb.527.

[4] Y. Xu, J. Liu, G. Ma, J. Wang, J. Lin, H. Wang, C. Zhang, M. Ding, Effect of iron loading on acidity and performance of Fe/HZSM-5 catalyst for direct synthesis of aromatics from syngas, Fuel 228 (2018) 1–9, https://doi.org/10.1016/j.fuel.2018.04.151.

[5] B. Zhao, P. Zhai, P. Wang, J. Li, T. Li, M. Peng, M. Zhao, G. Hu, Y. Yang, Y.-W. Li, Direct transformation of syngas to aromatics over Na-Zn-Fe5C2 and hierarchical HZSM-5 tandem catalysts, Chem 3 (2017) 323–333, https://doi.org/10.1016/j.chempr.2017.06.017.

[6] X. Yang, X. Su, D. Chen, T. Zhang, Y. Huang, Direct conversion of syngas to aromatics: a review of recent studies, Chin. J. Catal. 41 (2020) 561–573, https://doi.org/10.1016/S1872-2067(19)63346-2.

[7] R.A. Dagle, J.A. Lizarazo-Adarme, V. Lebarbier Dagle, M.J. Gray, J.F. White, D. L. King, D.R. Palo, Syngas conversion to gasoline-range hydrocarbons over Pd/ZnO/Al_2O_3 and ZSM-5 composite catalyst system, Fuel Process. Technol. 123 (2014) 65–74, https://doi.org/10.1016/j.fuproc.2014.01.041.

[8] S. Liu, A.C. Gujar, P. Thomas, H. Toghiani, M.G. White, Synthesis of gasoline-range hydrocarbons over Mo/HZSM-5 catalysts, Appl. Catal. A 357 (2009) 18–25, https://doi.org/10.1016/j.apcata.2008.12.033.

[9] H.M. Torres Galvis, J.H. Bitter, T. Davidian, M. Ruitenbeek, A.I. Dugulan, K.P. de Jong, Iron particle size effects for direct production of lower olefins from synthesis gas, J. Am. Chem. Soc. 134 (2012) 16207–16215, https://doi.org/10.1021/ja304958u.

[10] G. Yu, B. Sun, Y. Pei, S. Xie, S. Yan, M. Qiao, K. Fan, X. Zhang, B. Zong, Fe_xO_y@C spheres as an excellent catalyst for fischer-tropsch synthesis, J. Am. Chem. Soc. 132 (2010) 935–937, https://doi.org/10.1021/ja906370b.

[11] Y. Zhu, X. Pan, F. Jiao, J. Li, J. Yang, M. Ding, Y. Han, Z. Liu, X. Bao, Role of manganese oxide in syngas conversion to light olefins, ACS Catal. 7 (2017) 2800–2804, https://doi.org/10.1021/acscatal.7b00221.

[12] J. Zhang, S. Fan, T. Zhao, W. Li, Y. Sun, Carbon modified Fe-Mn-K catalyst for the synthesis of light olefins from CO hydrogenation, React. Kinet. Mech. Catal. 102 (2011) 437–445, https://doi.org/10.1007/s11144-010-0275-y.

[13] J. l Zhang, L.-h Ma, S.-b Fan, T.-S. Zhao, Y.-h Sun, Synthesis of light olefins from CO hydrogenation over Fe-Mn catalysts: Effect of carburization pretreatment, Fuel 109 (2013) 116–123, https://doi.org/10.1016/j.fuel.2012.12.081.

[14] S.A. Al-Sayari, Catalytic conversion of syngas to olefins over Mn-Fe catalysts, Ceram. Int. 40 (2014) 723–728, https://doi.org/10.1016/j.ceramint.2013.06.061.
[15] Y. Liu, F. Lu, Y. Tang, M. Liu, F.F. Tao, Y. Zhang, Corrigendum to "effects of initial crystal structure of Fe2O3 and Mn promoter on effective active phase for syngas to light olefin" [Appl. Catal. B: Environ. 261 (2020) 118219], Appl. Catal. B Environ. 278 (2020), 119287, https://doi.org/10.1016/j.apcatb.2019.118219.
[16] J.C. Park, S.C. Yeo, D.H. Chun, J.T. Lim, J.I. Yang, H.T. Lee, S. Hong, H.M. Lee, C. S. Kim, H. Jung, Highly activated K-doped iron carbide nanocatalysts designed by computational simulation for Fischer–Tropsch synthesis, J. Mater. Chem. A 2 (2014) 14371–14379, https://doi.org/10.1039/C4TA02413C.
[17] X. Yang, X. Su, B. Liang, Y. Zhang, H. Duan, J. Ma, Y. Huang, T. Zhang, The influence of alkali-treated zeolite on the oxide-zeolite syngas conversion process, Catal. Sci. Technol. 8 (2018) 4338–4348, https://doi.org/10.1039/C8CY01332B.
[18] B. Graf, H. Schulte, M. Muhler, The formation of methane over iron catalysts applied in Fischer-Tropsch synthesis A transient and steady state kinetic study, J. Catal. 276 (2010) 66–75, https://doi.org/10.1016/j.jcat.2010.09.001.
[19] P. Zhai, C. Xu, R. Gao, X. Liu, M. Li, W. Li, X. Fu, C. Jia, J. Xie, M. Zhao, X. Wang, Y.-W. Li, Q. Zhang, X.-D. Wen, D. Ma, Highly tunable selectivity for syngas-derived alkenes over zinc and sodium-modulated Fe_5C_2 catalyst, Angew. Chem. Int. Ed. 55 (2016) 9902–9907, https://doi.org/10.1002/anie.201603556.
[20] H.M.T. Galvis, J.H. Bitter, C.B. Khare, M. Ruitenbeek, A.I. Dugulan, K.P.D. Jong, Supported iron nanoparticles as catalysts for sustainable production of lower olefins, Science 335 (2012) 835–838, https://doi.org/10.1126/science.1215614.
[21] J. Xie, J. Yang, A.I. Dugulan, A. Holmen, D. Chen, K.P. de Jong, M.J. Louwerse, Size and promoter effects in supported iron fischer-tropsch catalysts: insights from experiment and theory, ACS Catal. 6 (2016) 3147–3157, https://doi.org/10.1021/acscatal.6b00131.
[22] X. Yang, T. Sun, J. Ma, X. Su, R. Wang, Y. Zhang, H. Duan, Y. Huang, T. Zhang, The influence of intimacy on the 'iterative reactions' during OX-ZEO process for aromatic production, J. Energy Chem. 35 (2019) 60–65, https://doi.org/10.1016/j.jechem.2018.11.003.
[23] J. Yang, E.Z. Tveten, D. Chen, A. Holmen, Understanding the effect of cobalt particle size on Fischer− tropsch synthesis: surface species and mechanistic studies by SSITKA and kinetic isotope effect, Langmuir 26 (2010) 16558–16567, https://doi.org/10.1021/la101555u.
[24] X. Yang, R. Wang, J. Yang, W. Qian, Y. Zhang, X. Li, Y. Huang, T. Zhang, D. Chen, Exploring the reaction paths in the consecutive Fe-based FT catalyst-zeolite process for syngas conversion, ACS Catal. 10 (2020) 3797–3806, https://doi.org/10.1021/acscatal.9b05449.
[25] J. Yang, D. Chen, A. Holmen, Understanding the kinetics and Re promotion of carbon nanotube supported cobalt catalysts by SSITKA, Catal. Today 186 (2012) 99–108, https://doi.org/10.1016/j.cattod.2011.10.026.
[26] V. Frøseth, S. Storsæter, Ø. Borg, E.A. Blekkan, M. Rønning, A. Holmen, Steady state isotopic transient kinetic analysis (SSITKA) of CO hydrogenation on different Co catalysts, Appl. Catal., A 289 (2005) 10–15, https://doi.org/10.1016/j.apcata.2005.04.009.
[27] B.C. Enger, V. Frøseth, J. Yang, E. Rytter, A. Holmen, SSITKA analysis of CO hydrogenation on Zn modified cobalt catalysts, J. Catal. 297 (2013) 187–192, https://doi.org/10.1016/j.jcat.2012.10.013.
[28] A. Carvalho, V.V. Ordomsky, Y. Luo, M. Marinova, A.R. Muniz, N.R. Marcilio, A. Y. Khodakov, Elucidation of deactivation phenomena in cobalt catalyst for Fischer-Tropsch synthesis using SSITKA, J. Catal. 344 (2016) 669–679, https://doi.org/10.1016/j.jcat.2016.11.001.
[29] C. Ledesma, J. Yang, E.A. Blekkan, A. Holmen, D. Chen, Carbon number dependence of reaction mechanism and kinetics in CO hydrogenation on a Co-based catalyst, ACS Catal. 6 (2016) 6674–6686, https://doi.org/10.1021/acscatal.6b01376.
[30] V.V. Ordomsky, Y. Luo, B. Gu, A. Carvalho, P.A. Chernavskii, K. Cheng, A. Y. Khodakov, Soldering of iron catalysts for direct synthesis of light olefins from syngas under mild reaction conditions, ACS Catal. 7 (2017) 6445–6452, https://doi.org/10.1021/acscatal.7b01307.
[31] Y. Liu, B.-T. Teng, X.-H. Guo, Y. Li, J. Chang, L. Tian, X. Hao, Y. Wang, H.-W. Xiang, Y.-Y. Xu, Y.-W. Li, Effect of reaction conditions on the catalytic performance of Fe-Mn catalyst for Fischer-Tropsch synthesis, J. Mol. Catal. A Chem. 272 (2007) 182–190, https://doi.org/10.1016/j.molcata.2007.03.046.
[32] C. Wang, Q.X. Wang, X.D. Sun, L.Y. Xu, CO hydrogenation to light alkenes over Mn/Fe catalysts prepared by coprecipitation and sol-gel methods, Catal. Lett. 105 (2005) 93–101, https://doi.org/10.1007/s10562-005-8011-3.
[33] Q. Chen, W. Qian, H. Zhang, H. Ma, Q. Sun, W. Ying, Effect of Li promoter on FeMn/CNTs for light olefins from syngas, Catal. Commun. 124 (2019) 92–96, https://doi.org/10.1016/j.catcom.2019.03.010.
[34] S. Lyu, L. Wang, Z. Li, S. Yin, J. Chen, Y. Zhang, J. Li, Y. Wang, Stabilization of ε-iron carbide as high-temperature catalyst under realistic Fischer–Tropsch synthesis conditions!Abstract, 6219-6219, Nat. Commun. 11 (2020) 6219, https://doi.org/10.1038/s41467-020-20068-5.
[35] Y. Xu, P. Zhai, Y. Deng, J. Xie, X. Liu, S. Wang, D. Ma, Highly selective olefin production from CO(2)hydrogenation on iron catalysts: a subtle synergy between manganese and sodium additives, Angew. Chem. Int. Ed. 59 (2020) 21736–21744, https://doi.org/10.1002/anie.202009620.
[36] K. Yuan, Z. Bing, J.Z. Niu, S.B. Li, H.L. Wang, T. Tanaka, S. Yoshida, Amorphous features of working catalysts: XAFS and XPS characterization of $Mn/Na_2WO_4/SiO_2$ as used for the oxidative coupling of methane, J. Catal. 173 (1998) 399–408, https://doi.org/10.1006/jcat.1997.1900.
[37] Y. Liu, J.F. Chen, J. Bao, Y. Zhang, Manganese-modified Fe_3O_4 microsphere catalyst with effective active phase of forming light olefins from syngas, ACS Catal. 5 (2015) 3905–3909, https://doi.org/10.1021/acscatal.5b00492.
[38] M. Ding, Y. Yang, J. Xu, Z. Tao, H. Wang, H. Wang, H. Xiang, Y. Li, Effect of reduction pressure on precipitated potassium promoted iron–manganese catalyst for Fischer–Tropsch synthesis, Appl. Catal., A 345 (2008) 176–184, https://doi.org/10.1016/j.apcata.2008.04.036.
[39] I.K. van Ravenhorst, C. Vogt, H. Oosterbeek, K.W. Bossers, J.G. Moya-Cancino, A. P. van Bavel, A.M.J. van der Eerden, D. Vine, F.M.F. de Groot, F. Meirer, B. M. Weckhuysen, Capturing the genesis of an active fischer-tropsch synthesis catalyst with operando X-ray nanospectroscopy, Angew. Chem. Int. Ed. 57 (2018) 11957–11962, https://doi.org/10.1002/anie.201806354.
[40] Q. Chang, C. Zhang, C. Liu, Y. Wei, A.V. Cheruvathur, A.I. Dugulan, J. W. Niemantsverdriet, X. Liu, Y. He, M. Qing, L. Zheng, Y. Yun, Y. Yang, Y. Li, Relationship between iron carbide phases (epsilon-Fe_2C, Fe_7C_3, and chi-Fe_5C_2) and catalytic performances of Fe/SiO_2 fischer-tropsch catalysts, ACS Catal. 8 (2018) 3304–3316, https://doi.org/10.1021/acscatal.7b04085.
[41] E. de Smit, A.M. Beale, S. Nikitenko, B.M. Weckhuysen, Local and long range order in promoted iron-based Fischer-Tropsch catalysts: a combined in situ X-ray absorption spectroscopy/wide angle X-ray, J. Catal. 262 (2009) 244–256, https://doi.org/10.1016/j.jcat.2008.12.021.
[42] B. Chen, D. Wang, X. Duan, W. Liu, Y. Li, G. Qian, W. Yuan, A. Holmen, X. Zhou, D. Chen, Charge-tuned CO activation over a chi-Fe5C2 Fischer-Tropsch catalyst, ACS Catal. 8 (2018) 2709–2714, https://doi.org/10.1021/acscatal.7b04370.
[43] M. Zhang, J. Ren, Y. Yu, Insights into the hydrogen coverage effect and the mechanism of Fischer-Tropsch to olefins process on Fe_5C_2 (510), ACS Catal. 10 (2020) 689–701, https://doi.org/10.1021/acscatal.9b03639.
[44] M. Oschatz, T.W. van Deelen, J. Weber, W.S. Lamme, G. Wang, B. Goderis, O. Verkinderen, A. Dugulan, K.P.De Jong, Effects of calcination and activation conditions on ordered mesoporous carbon supported iron catalysts for production of lower olefins from synthesis gas, Catal. Sci. Technol. 6 (2016) 8464–8473, https://doi.org/10.1039/C6CY01251E.
[45] Q. Yang, X.-P. Fu, C.-J. Jia, C. Ma, X. Wang, J. Zeng, R. Si, Y.-W. Zhang, C.-H. Yan, Structural determination of catalytically active subnanometer iron oxide clusters, ACS Catal. 6 (2016) 3072–3082, https://doi.org/10.1021/acscatal.6b00328.
[46] J.M. Gracia, F.F. Prinsloo, J.W. Niemantsverdriet, Mars-van krevelen-like mechanism of CO hydrogenation on an iron carbide surface, Catal. Lett. 133 (2009) 257–261, https://doi.org/10.1007/s10562-009-0179-5.
[47] M.O. Ozbek, J.W. Niemantsverdriet, Methane, formaldehyde and methanol formation pathways from carbon monoxide and hydrogen on the (001) surface of the iron carbide chi-Fe_5C_2, J. Catal. 325 (2015) 9–18, https://doi.org/10.1016/j.jcat.2015.01.018.